doi:10.3788/gzxb20184701.0112004

GSSM 缩比模型子孔径拼接误差分析

安其昌[1,2],张景旭[1],杨飞[1],赵宏超[1]
(1 中国科学院长春光学精密机械与物理研究所,长春 130033)
(2 中国科学院大学,北京 100039)

摘 要:巨型科学可控反射镜(GSSM)缩比模型(GSSMP)的子孔径拼接误差的分析可以指导 GSSM 的面形检测工作.GSSMP 子孔径拼误差包括子孔径刚体位移误差以及中频扰动.对子孔径刚体位移误差而言,合理的靶标布置以及最小二乘算法的使用,可将误差量级降低到计算机可分辨的最低程度,即不引入算法误差;同时也降低了对测试执行部件的精度要求.对中频扰动误差而言,可结合标准平面镜与干涉仪对实验环境中大气湍流的影响进行估计.除此之外,对子孔径拼接顺序带来的误差进行分析.最后,基于三十米望远镜的面形评价方法,即斜率均方根对上述误差进行换算表征.算法修正后,子孔径对准误差为 10^{-6} μrad、子孔径平移误差为 10^{-6} μrad、子孔径倾斜误差为 10^{-6} μrad 以及大气扰动误差为 0.04 μrad.利用信噪比来表征拼接顺序所带来的影响,使用一个子孔径作为基准进行拼接的情况下,拼接顺序带来的影响小于 2%.本文的拼接算法,可以在较低的机械精度下,利用靶标对准与合理的拼接顺序,达到较高的拼接精度.

关键词:三十米望远镜;巨型科学可控反射镜原理样机;误差分析;子孔径拼接
中图分类号:TH751 **文献标识码**:A **文章编号**:1004-4213(2018)01-0112004-13

Giant Science Steering Mirror Prototype Sub-aperture Testing Error Analysis

AN Qi-chang[1,2], ZHANG Jing-xu[1], YANG Fei[1], ZHAO Hong-chao[1]
(1 *Changchun Institute of Optics, Fine Mechanics and Physics, Chinese Academy of Sciences, Changchun* 130033, *China*)
(2 *Graduate University of Chinese Academy of Sciences, Beijing* 100039, *China*)

Abstract: Giant Steerable Science Mirror (GSSM) is largest flat mirror as the tertiary mirror of Thirty Meter Telescope (TMT). To evaluate the performance of GSSM under gravity load, the mirror figure needs to be tested. Erorr analysis is the most imortant step for the reliability of metrology. For its large size and plate character, Sub aperture stitching will be used to reach the full aperture figure. GSSMP is the prototype of GSSM. Research on GSSMP sub aperture testing error will help understanding and learning how to build GSSM. The stitching error is divided into two parts: rigid body location error and middle frequency turbulence. According to each part, theoretical analysis and experience have been done drawing the conclusion that the algorithm with probable marks will suppress rigid body error efficiently and the influence of the turbulence is achieved by smaller aperture system and interferometer. What is more, stitching order is also related to stitching order. Using one reference aperture and fitting other apertures onto it allow introducing least error to the final result. All the performance is specified by Slope

Foundation item: The Youth Innovation Promotion Association CAS(No.2016198), the National Natural Science Foundation of China (Nos. 11403022,11673080)
First author: AN Qi-chang(1988-),male, Ph.D. candidate, research assistant, mainly focuses on large aperture telescope testing and so on. Email:anjj@mail.ustc.edu.cn
Supervisor (Contact author): ZHANG Jing-xu (1964-), male, professor, Ph.D., mainly focuses on large telescope design. Email:Zhangjx@ciomp.ac.cn
Received: Dec.26, 2016; **Accepted**: Mar.10, 2017

RMS, which is required by TMT. After fitting, Shift error is 10^{-6} μrad, Piston error is 10^{-6} μrad, Tip/tilt error is 10^{-6} μrad and Air turbulence is 0.04 μrad. The error involved by the rigid body is ignorable, and the air turbulence is 3nm in RMS. By Slope MS, the reqiured metric of TMT, the influence of stitching error will be discussed and the orders chosen here did not increase the Signal to Noise ratio significantly in the figure at the level of 2%. Here the conclution was drawed that feature will help a lot in lowering the stitching error.

Key words: Thirty Meter Telescope; Giant steerable science mirror prototype; Error analysis; Sub aperture stitching

OCIS Codes: 120.4640; 120.4610; 120.4800; 120.5050

0 Introduction

Thirty Meter Telescope (TMT) is one of the largest telescopes in this world. Changchun Institute of Optics, Fine Mechanics and Physics, Chinese Academy of Sciences (CIOMP) takes charge of the tertiary mirror, noted as the Giant Steerable Science Mirror (GSSM, in shot). The 3.594 m×2.576 m flat mirror will point the instruments on the Science platform during the telescope tracing[1-3].

GSSM is one of the most complicated steering mirror systems in the world. The largest segmented telescopes under construction (E-ELT, TMT) both have steering mirror in their main optical systems. ELT M5 is a fast steering mirror to direct the beam form M1 to the instruments below. Meanwhile, the steering mirror in TMT is tertiary mirror. When the main telescope tracking the stallers, GSSM will do the rotating and tilting to guide the light beam form M2 to the science instruments on the Science plates. Thus the tertiary mirror is also called Giant Science Steering Mirror.

Single sub aperture metrology aberration Δ_{sub} is cumulated and enlarged according to rull aperture radius R and sub aperture diameter d_{s}, as $\Delta_{\mathrm{sub}} \propto d_{\mathrm{s}}^2/8R$.

The error is quadratic depended on sub aperture size. However, the number of sub apertures is approximated as follows. So, it is a coupled procedure to consider sub aperture feature[4-10], $N_{\mathrm{sub}} \propto R^2/2d_{\mathrm{s}}^2$.

GSSM mirror support system will be carefully designed and adjusted to keep the mirror figure during telescope motion. The mirror figure will be evaluated by Plate Scale Error and Slope RMS. GSSM mirror specification will is divided into two parts, one is the Plate Scale error (combined by power and astigmatism), and the other one is Slope RMS (relative to middle frequency ripple)[11-14]. Considering the GSSM mirror is too big for almost all the plate interferometers, the mirror figure will be evaluated by stitched aperture.

In the very early age, by measuring the Zernike coefficient of discrete sub aperture, the low order components of full aperture was estimated. The essential problem is losing the higher component. Around the very beginning of 20th century, overlapping the sub apertures realized metrology of mirror figure. With the growing size of telescope, timing and cost for measuring large mirror figure increased dramatically. Peng Su in Arizona Universe invested maximum likelihood estimation to figure out the low order component without full stitched aperture[8-10].

Up to now, GSSM is one of the largest flat mirror in the world. To better understand the requirement and ensure the GSSM will be successfully completed, TMT and CIOMP decided to contribute a 1/4 scaled prototype (Giant Science Steering Mirror Prototype, GSSMP). The mirror of GSSMP is 894 mm×654 mm ×12 mm and its size is much larger than the plate interferometer (600 mm in circle) in our instrument, so it is necessary to process sub aperture stitching. Furthermore, the construction of Prototype is focused on leaning and understanding. Full size tertiary mirror figure testing will only be realized by stitching, so the experience is also very valuable for the following work[15-17].

Due to the giant size of GSSM, the error analysis comes to be very important but complicated. Before assembling with main telescope, no way to check the mirror except stitching method. The error analysis helps the system engineers to allocation the accuracy of the facility used in testing (guide, motor, encoder, etc.), and the final metric for metrology itself. The concrete testing procedure is also determined by the error analysis[18-21].

All the performance is specified based on Slope RMS, which is required by TMT. Rigid body location

error and middle frequency turbulence is investigated to evaluate the stitching. Signal to Noise ratio is considered for choosing stitching order, and one fiducial aperture was used to reduce the error.

1 Principle for stitching error

Sub-aperture stitching had developed from the discrete-aperture method to the over-lapped aperture method. For GSSMP, as shown in Fig.1, four overlapped sub-apertures were set realizing reconstruction of the full aperture mirror figure. The sub-aperture is arranged in the form that both 'circling' and 'parallel' mods will realize the feature, adapting to different testing hardware.

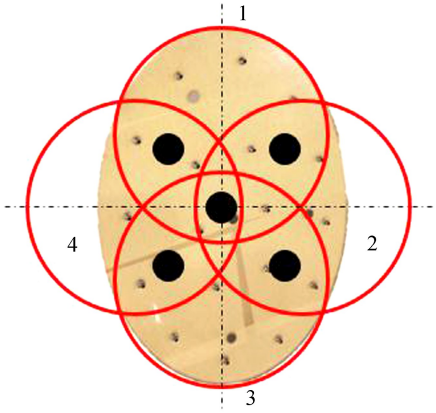

Fig.1 Allocation of the sub-apertures for GSSMP

GSSM/GSSMP mirror figure specification is very different from the normal case. The procedure for the specification is circling the ellipse figure, toking out the low Frequency part as Plate Scale error and calculating the RMS of residual figure slope. The first step is circling the ellipse aperture and then removing the power and astigmatism. The slope RMS is the root mean square of mirror surface slope strongly depending on the middle frequency components.

As stitching, there are in total three kinds of error will be take into condition including the shift error between the two sub apertures under stitching, the piston and tip/tilt error between them, and the turbulence(mainly coming from seeing the lab, vibration, noise in detectors etc.). Thus, the stitching error can be expressed as follows.

$$\Delta_{\text{stitching}}(x,y)=P+T_x x+T_y y+S_x\frac{\partial\Phi(x,y)}{\partial x}+S_y\frac{\partial\Phi(x,y)}{\partial y}+n \tag{1}$$

Here we note, P is the coefficient for piston error, T_x and T_y is the coefficient for tip/tilt error, S_x and S_y is the coefficient for shifting error, n refers to turbulence. Here, the error sources will be discussed separately, checking whether or not these error can be sufficiently suppressed.

Location of the marks shall be discussed previous to the analysis. Feature of the marks will determine the accuracy of the stitching procedure. Basically, in the overlap section, there at least one market to help locating the sub-apertures. Different to aspheric mirror, where the distortion will play a larger role in error budget, the flat mirror stitching testing will not involve distortion. So, in the testing, only one mark will be located in the overlap range.

The verification experience was done in an alternative way. First the reflecting mirror will be tested in full aperture and its figure was regarded as the ideal reference of stitching. Then, an aperture was inserted to the beam only allowing the light beam coming though partly. As moving the aperture, the interferometer will adjust the pointing angle and position alone the light axis direction, simulating the mechanical error during the motion of the sub aperture testing. To simplify this testing, numeral simulation will also realize the verification by cutting the full aperture into several small circle ones. Mechanical error was represented by tipping and powering the data mathematically.

It is similar to the marks. Marks on the mirror allow lowing the accuracy of mechanical parts. There are two alternative ways to verify the effect. One option is actually locate the feature and the anther one is to do this numerally. The measurement is shown in the left panel of Fig.3. Sketch of the verification test basic specification is shown in the right panel of Fig.2.

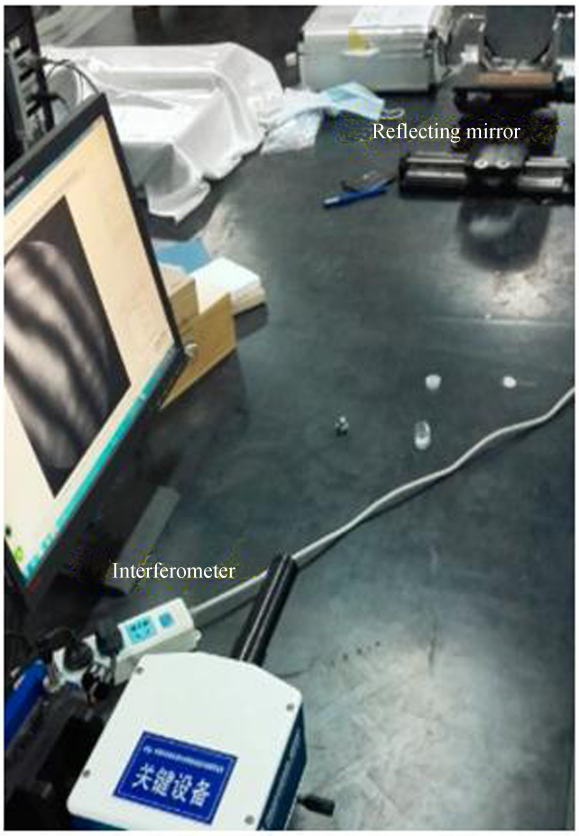

Measurement set up

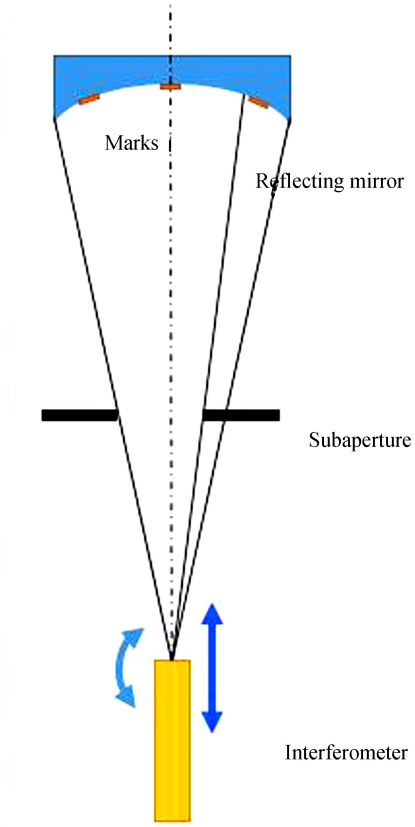

Verification test basic specification

Fig.2 Sketch of sub aperture testing

In the following, the stitching order influence will be under discussion.

Sub aperturs of GSSMP will be combided in a certain sequence. Two subapertures to be stitched are notes as $S_{Ti}(m,n)$ and $S_{Tj}(m,n)$. Overlapping section is rectangle of $M\times N$. $S_{\text{ideal}}(m,n)$ presents the ideal actual data in covered section. Δ_{ij} is stitching error, where $m\in[1,M], n\in[1,N]$.

The stitching error can be presented by the following formula.

$$\Delta_{ij}=\frac{1}{MN}\sum_{m=1,n=1}^{m=M,n=N}[S_{Ti}(m,n)-S_{Tj}(m,n)]=$$
$$\frac{1}{MN}\sum_{m=1,n=1}^{m=M,n=N}[S_{Ti}(m,n)-S_{\text{ideal}}(m,n)-S_{Tj}(m,n)+S_{\text{ideal}}(m,n)]$$

Squaring two sides of the formula, here is that

$$\Delta_{ij}^2=\frac{1}{MN}(\sigma_{Ti}^2+\sigma_{Tj}^2)$$

The first method is stitching the aperture one by one in turn. Taking GSSMP as example, the order of stitching is 1→2, 2→3, 3→4. Square of the error is presented as follows, where P is the number of sub-apertures.

$$\Delta_1^2=\frac{1}{MN}\sum_{j=2}^{P}(\sigma_{T1}^2+\sigma_{Tj}^2)=\frac{1}{MN}\left(P\sigma_{T1}^2+\sum_{j=2}^{P}\sigma_{Tj}^2\right) \tag{2}$$

The second method is stitching the aperture every two appertures then conbiming them together. Taking GSSMP as example, the order of stitching is 1→2, 3→4, 1&2→3&4. The square of the error is presented as follows, where P is the number of sub-apertures.

$$\Delta_2^2=\frac{1}{MN}\sum_{j=1}^{P-1}(\sigma_{Tj}^2+\sigma_{Tj+1}^2)=\frac{1}{MN}\left(2\sum_{j=2}^{P}\sigma_{Tj}^2+\sigma_{T1}^2+\sigma_{TP}^2\right) \tag{3}$$

The third method is stitching the apertures to one certain basic aperture. Taking GSSMP as example, the order of stitching is 1→2, 1→3, 1→4. The square of error is presented as follows, where P is the number of sub-apertures.

$$\Delta_3^2=\frac{1}{MN}\left[\sum_{j=2}^{P}(\sigma_{T1}^2+\sigma_{Tj}^2)-\sum_{j=2}^{P}(\sigma_{T1}^2)\right] \tag{4}$$

Here, the distribution of the error is supposed to be the same, and the standard deviation is noted as σ^2.

$$\sigma_{Tj}^2=\sigma^2$$

Simplifying Eq.(2) to Eq.(4), square of the error are re-write as follows, where P is the number of sub-apertures.

Setting $S_{\mathrm{RMS}}^2=\frac{\sigma^2}{MN}$ as the squared unique slope RMS.

$$\Delta_1^2=PS_{\mathrm{RMS}}^2 \tag{5}$$

$$\Delta_2^2=2P\sigma^2S_{\mathrm{RMS}}^2 \tag{6}$$

$$\Delta_3^2=S_{\mathrm{RMS}}^2 \tag{7}$$

Comparing the Eq.(5) and Eq.(7), they specify the relationship between the stitching with and without one based aperture. When the number of sub-apertures increase, stitching error with a based aperture is smaller than the case without base, where P is the number of sub-apertures.

$$\Delta_3^2\sim\frac{1}{P}\Delta_1^2$$

As stated earlier, subaperture stitching mainly suffers from at least one of the following four error sources: shifting error, piston error, tip/tilt error, turbulence.

GSSMP is under specification of Plate Scale error and Slope Root Mean Square(Slope RMS, in short),as shown in Fig.2.

Plate Scale is relatived to power and astigmatism. Here, the figure in subaperture is the same and equaly presented by Zernike polynomials in covered section,as shown in Fig.3.

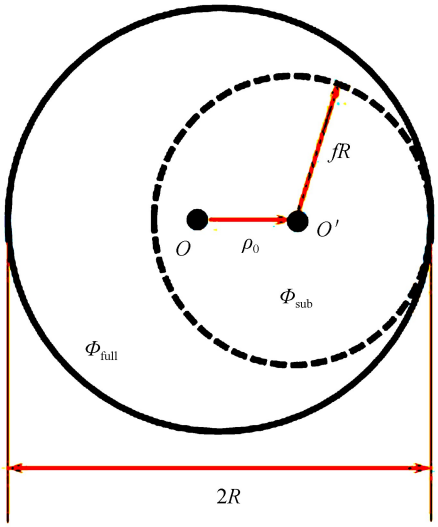

Fig.3 Sub aperture and full aperture share the same figure

$$\Phi_{\mathrm{sub}}(\rho,\theta)=\Phi_{\mathrm{full}}(\rho',\theta')=\sum_{j=4}^{N_m}a_jZ_j(\rho',\theta')=\sum_{j=4}^{N_m}b_jZ_j(\rho,\theta)$$

Considering the power term firstly, the RMS in a sub aperture with fR radius is as following

$$\sigma_{\mathrm{s-power}}^2=\frac{\alpha^2}{3}R^4f^4+\frac{\rho_0^2-\overline{\Phi}_{\mathrm{s-power}}}{2}(\alpha R^2f^2+\rho_0^2-\overline{\Phi}_{\mathrm{s-power}})$$

Noting the mean value at this section is

$$\overline{\Phi}_{\mathrm{s-power}}=\frac{\alpha}{2}R^2f^2+\alpha\rho_0^2 \tag{8}$$

Here R was the radius of the full aperture; fR was the radius of sub aperture; ρ_0 was the distance between sub aperture center and full aperture center.α was the coefficient of power term in full aperture.

It is similar for astigmatism term, and the RMS in a sub aperture with fR radius is as following

$$\sigma_{\mathrm{s-astig}}^2=\frac{\beta^2}{6}R^4f^4+\beta^2\rho_0^2R^2f^2$$

Noting the mean value at this section is

$$\overline{\Phi}_{\mathrm{s-astig}}=\beta\rho_0^2\sin(2\theta) \tag{9}$$

Here, R was the radius of the full aperture; fR was the radius of sub aperture; ρ_0 was the distance between sub aperture center and full aperture center. β was coefficient of astigmatism term in full aperture.

$$\sigma_{\mathrm{f-power}}^2=\frac{1}{12}\alpha^2R^4$$

Noting the mean value at this section is

$$\overline{\Phi}_{\text{f-power}}=\frac{1}{2}\alpha R^2$$

Here, R was the radius of the full aperture; fR was the radius of sub aperture; ρ_0 was the distance between sub aperture center and full aperture center.α is the coefficient of power term in full aperture.

$$\sigma^2_{\text{f-astig}}=\frac{\beta^2}{6}R^4$$

Noting the mean value at this section is

$$\overline{\Phi}_{\text{f-astig}}=0$$

Here, R was the radius of the full aperture; fR was the radius of sub aperture; ρ_0 was the distance between sub aperture center and full aperture center. β was coffen of astigmatism term in full aperture.

$$\sigma^2_{\text{s-power}}+2\sigma^2_{\text{s-astig}}=\frac{\alpha^2+4\beta^2}{12}R^4f^4+\frac{(1+\alpha)^2\rho_0^4+4\beta^2\rho_0^2R^2f^2}{2}$$

Here, R the radius of the full aperture; fR the radius of sub aperture; ρ_0 is the distance between sub aperture center and full aperture center. α is the coefficient of power term in full aperture. β is coffen of astigmatism term in full aperture.

For the full aperture

$$\sigma^2_{\text{f-power}}+2\sigma^2_{\text{f-astig}}=\frac{\alpha^2+4\beta^2}{12}R^4 \tag{10}$$

Here, R was the radius of the full aperture. fR was the radius of sub aperture. ρ_0 was the distance between sub aperture center and full aperture center. α is the coefficient of power term in full aperture.

Error in Plate Scale calculation considering the

$$E_{\text{PalteScale}}=\frac{(1+\alpha)^2\rho_0^4+4\beta^2\rho_0^2R^2f^2}{2} \tag{11}$$

Plate scale error will follow a law of $(\rho_0^2+1)^2$.

For higher order, maybe at the same level of air turbulence, it follows a $f^{5/3}$ law. It will not influence Plate scale error and it will interaction with slope RMS calculation.

$$\sigma_s^2=f^{\frac{5}{3}}\sigma_f^2 \tag{12}$$

Here, the influence of air turbulence will be presented here. Optical path difference $\text{OPD}(x,y,t)$ is defined as formula (1)3, assuming light transmitting along Z axis

$$\text{OPD}(x,y,t)=\int_0^L n(x,y,z,t_i)\,\text{d}z \tag{13}$$

$n(x,y,x,t_i)$ noting air index at location (x,y,z); $\text{d}z$ is small distance along Z; L the thickness light passing though; t_i discrete time series($i=1\cdots N$).

Slope of the wave front is presented by Eq.(14).

$$\text{slope}_x(x,y,t_i)=\frac{\partial}{\partial x}\text{OPD}(x,y,t_i)=\frac{\partial}{\partial x}\int_0^L n(x,y,z,t_i)\,\text{d}z \tag{14}$$

$n(x,y,x,t_i)$ noting air index at location (x,y,z); $\text{d}z$ is small distance along Z; L the thickness light passing though; t_i discrete time series ($i=1\cdots N$).

Light is considered transmitting through every piece of air with different index, and reflecting at the flat mirror. Folding the light path allows simplification of its calculation, as shown in Fig.4.

The input angle at first layer θ_1; index at left n_0,index at right n_1; output angle at first layer θ_1'; the input angle at second layer θ_2, output angle θ_2'; index at left n_1; index at right n_2; the input angle at third layer θ_3; output angleθ_3'; index at left n_2;

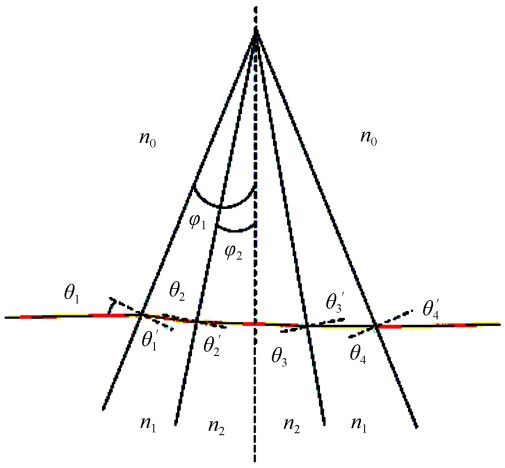

Fig.4 Index difference specification

index at right n_1; the input angle at fourth layer θ_4; output angle θ_4'; index at left n_2; index at right n_0; the two layers are tipped by φ_1 and φ_2.

When the angle is small the relationship is approximated as follows

$$\theta_1' n_1 = \theta_1 n_0, \theta_2' n_2 = \theta_2 n_1, \theta_3' n_1 = \theta_3 n_2, \theta_4' n_0 = \theta_4 n_1$$

Considering

$$\theta_2 = \theta_1' - (\varphi_1 - \varphi_2)$$
$$\theta_3 = 2\varphi_2 - \theta_2'$$
$$\theta_4 = \theta_3' - (\varphi_1 - \varphi_2)$$

The difference between he input angle and output angle $\Delta\theta$ is as shown in follows

$$\Delta\theta = \theta_4' - \theta_1 = \frac{n_1}{n_0}\left[\frac{\left(2\varphi_2 - \frac{n_0\varphi_1 - n_1(\varphi_1 - \varphi_2)}{n_2}\right)n_2}{n_1} + \varphi_1 - \varphi_2\right] - \varphi_1 = \frac{2}{n_0}[\varphi_1(n_1 - n_0) + \varphi_2(n_2 - n_1)]$$

where $n_0 = 1$, it will come to the N th layer, the angular change is as Eq.(15).

$$\Delta\theta_{\text{total}} = \sum_{i=1}^{N} 2\Delta n_i \varphi_i \tag{15}$$

Noting $\Delta n_i = n_{i-1} - n_i, (i = 1, 2, \cdots, N), \varphi_i$ is the light bending in the air at layer i

Reforming the Eq.(15)

$$\Delta\theta_{\text{total}} = \sum_{j=1}^{N}\sum_{i=1}^{N} 2\Delta n_i \varphi_i - \sum_{j=1}^{N-1}\sum_{i=1}^{N} 2\Delta n_i \varphi_i$$

Considering

$$2fR\varphi_i = dz_i$$

where fR the radius of sub aperture, $\mathrm{d}z_i$ the thickness of i th layer.

$$2fR\Delta\theta_{\text{total}} = \sum_{j=1}^{N}\sum_{i=1}^{N} 2\Delta n_i \mathrm{d}z_i - \sum_{j=1}^{N-1}\sum_{i=1}^{N} 2\Delta n_i \mathrm{d}z_i = \sum_{j=1}^{N} n_i \mathrm{d}z_i - \sum_{j=1}^{N-1} n_i \mathrm{d}z_i = \mathrm{diff}(\mathrm{OPD})$$

Where diff $(\bullet)$ is refer to difference calculation of OPD (x, y, t), Power Spectrum of series $[x_1, x_2, \cdots, x_N]$ is shown as follows

$$\mathrm{PSD} = \frac{1}{2\pi N}\left|\sum_{i=1}^{N} x_i \mathrm{e}^{-\mathrm{j}\omega}\right|^2$$

ω is in rad/s, and $i = 1 \cdots N$.

Power Spectral density is of optical path difference series and Slope series is shown as (16).

$$\begin{cases}\mathrm{PSD}_{\mathrm{OPD}} = \dfrac{1}{2\pi N}\left|\displaystyle\sum_{i=1}^{N} \mathrm{OPD}(x, y, t_i)\,\mathrm{e}^{\frac{2\pi\mathrm{j}kt}{N}}\right|^2 \\ \mathrm{PSD}_{\mathrm{slope}} = \dfrac{1}{2\pi N}\left|\displaystyle\sum_{i=1}^{N} \mathrm{slope}_x(y, t_i)\,\mathrm{e}^{\frac{2\pi\mathrm{j}kti}{N}}\right|^2\end{cases} \tag{16}$$

Reforming Eq.(17)

$$E_{\mathrm{SlopeRMS}} = \sum \mathrm{PSD}_{\mathrm{slope}} = \sum_{k=1}^{N}\left(\frac{2\pi k}{N}\right)^2 \mathrm{PSD}_{\mathrm{OPD}} \tag{17}$$

Influence of air turbulence on slope RMS is shown in Eq.17. This will realize the estimation of slope measurement error by an interferometer. This small sampling aperture is easy to be accessed to by the margin part of large plate interferometer.

2 Numeral analysis for stitching error

Analytically, the two subapertures under sttching will be pricisely positioned ensuring the pixels in overlpaing area aligned to the counter one. Marks are used to improve the stitching accuracy. The marks are located such that every overlapping section contain one. After transition using the marks, the residual error is shifting error. The order of the error may be equal to the diametion of several pixels. Stiching error is specified in Table 1. The error is too tiny and very close to the numeral limitation of MATLAB.

The piston and tip/tilt error, namely, rigid body error, is also considered. A sub aperture is set as basic in the left panel of Fig.5. As shown in the right panel of Fig.5, rigid body error is added to a nearby sub aperture. The stitching result is shown in the Fig.6, the error is mainly suppressed, and the result is

Table 1 Stitching error @ only shift considered

	RMS of the full aperture/slope RMS	RMS of the stitched aperture/slope RMS	Residual error of the stitching
1	0.24 μrad	0.24μrad	10^{-6}
2	0.88 μrad	0.88 μrad	10^{-6}
3	0.35 μrad	0.35 μrad	10^{-6}
4	0.13 μrad	0.13 μrad	10^{-6}
5	0.16 μrad	0.16 μrad	10^{-6}

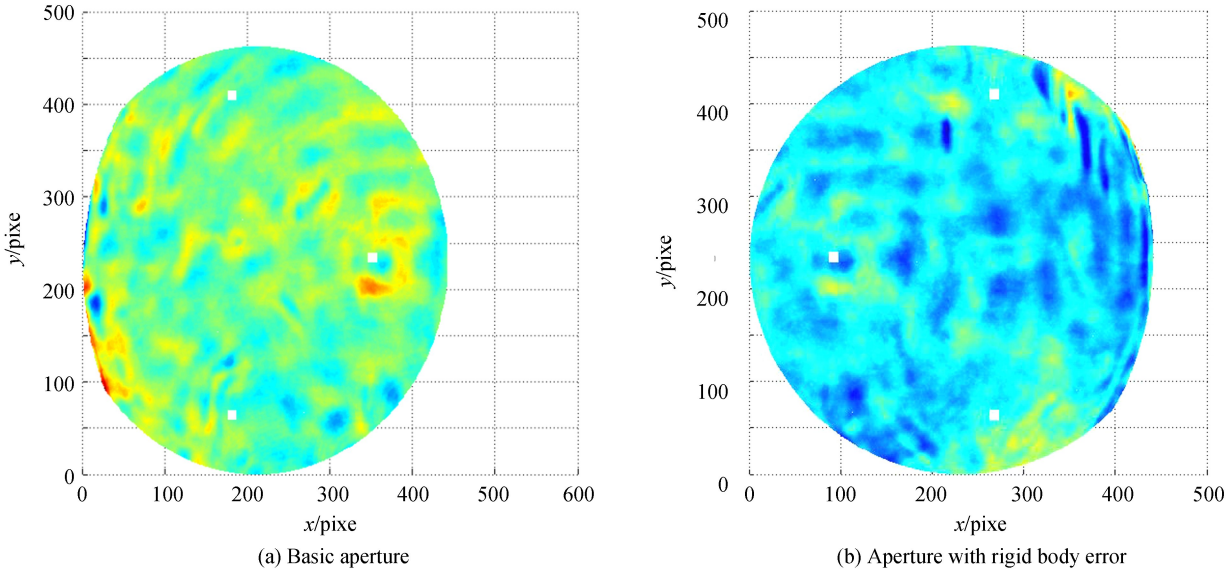

Fig.5 Influence of rigid body motion on stitching

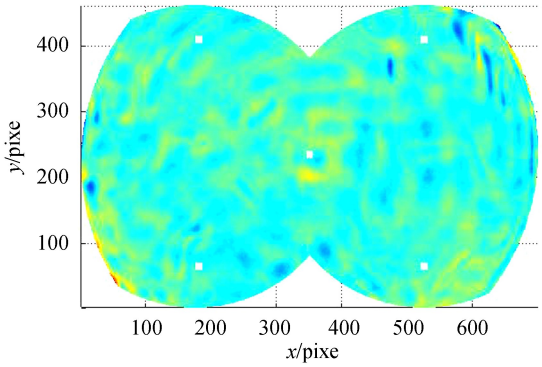

Fig.6 Sub aperture stitching result for rigid body error

shown in the Table 2. After fitting with least square method, the error resulted by rigid body motion is very tiny. This conduction is very important, for it can loose the accuracy requirement of testing instrument. Motion accuracy of the testing instrument contribute very little to the final result with the help of marks.

Table 2 Result of the sub aperture stitching with rigid body error

	RMS of the full aperture/slope RMS	RMS of the stitched aperture/slope RMS	Residual error of the stitching
1	0.56 μrad	0.56 μrad	10^{-6}
2	0.69 μrad	0.69 μrad	10^{-6}
3	0.38 μrad	0.38 μrad	10^{-6}
4	0.57 μrad	0.57 μrad	10^{-6}
5	0.29 μrad	0.29 μrad	10^{-6}

The turbulence was also taken into condition. To make it easy, the turbulence is considered as white noise. A sub aperture is set as basic as shown in the left panel of Fig.7. As shown in the right panel of Fig.7, subaperture is added with white noise. The residual error is shown in the Fig.8. Least squaring

fitting realizes supression of almost all the low order abberation , meanwhile, the white noise is still left.

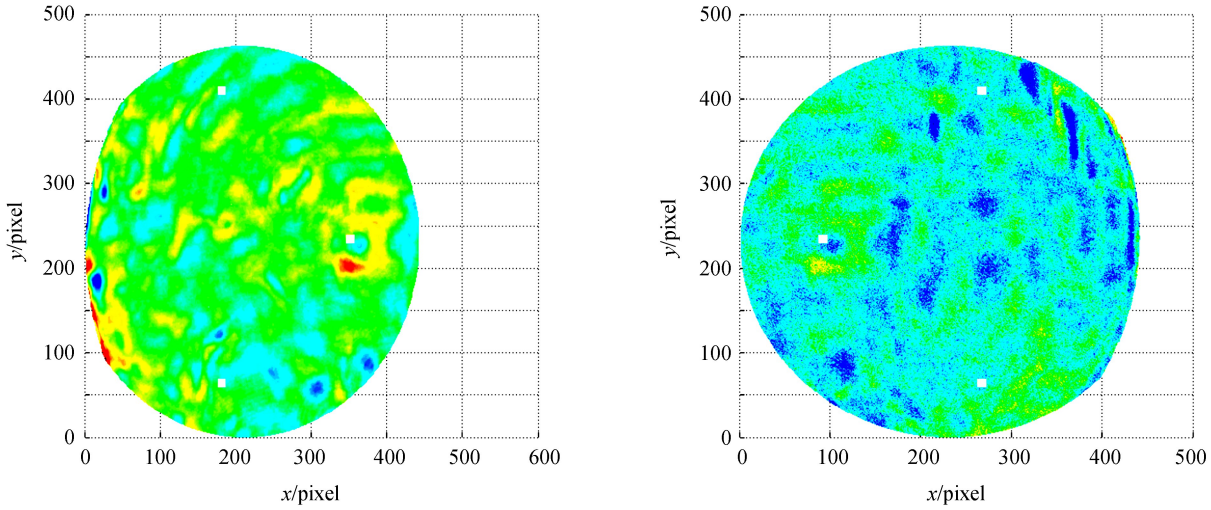

(a) Basic aperture (b) Aperture with white noise error

Fig.7 Influence of white noise on stitching

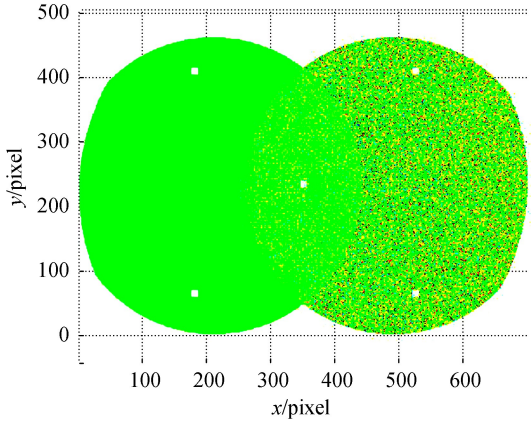

Fig.8 Stitching residual error with white noise error

Here, the middle frequency turbulence is also considered. The middle frequency noise is dominated by the air turbulence. A sub aperture is set as basic shown in the left panel of Fig.9, and sub aperture under stitching with air turbulence is shown in the right panel of Fig.9. The residual error is shown in Fig.10 and Table 3.

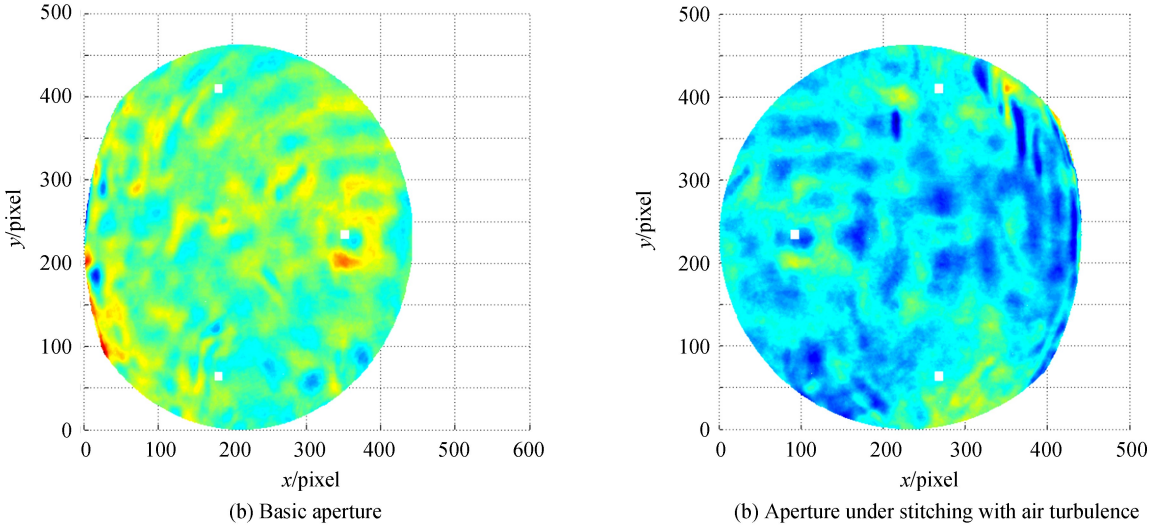

(b) Basic aperture (b) Aperture under stitching with air turbulence

Fig.9 Influence of air turbulence on stitching

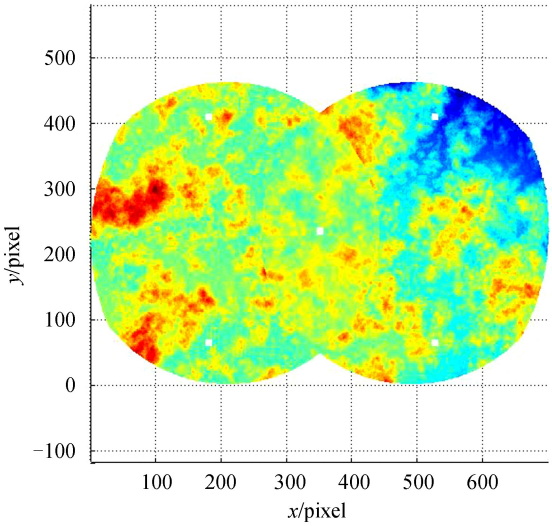

Fig.10 Stitching residual error with air turbulence

Table 3 Residual error after adding turbulence

	Added random error/slope RMS	Added middle frequency error slope RMS	Residual random error/slope RMS	Residual middle frequency error/slope RMS
1	0.53 μrad	0.46 μrad	0.53 μrad	0.46 μrad
2	0.57 μrad	0.48 μrad	0.57 μrad	0.48 μrad
3	0.72 μrad	0.41 μrad	0.72 μrad	0.41 μrad
4	0.84 μrad	0.17 μrad	0.84 μrad	0.17 μrad
5	0.43 μrad	0.92 μrad	0.43 μrad	0.92 μrad

Measurement the figure of smaller mirror some distance from interferometer realizing the estimation for amount of air turbulence. The mirror is previously tested very close to the interferometer. The mirror figure tested in this case is set as the reference. As the mirror is tested in longer distance, the figure combined with the air turbulence will be recorded. Analyzing data in smaller aperture allows specifying the error involved by air turbulence.

The testing result is shown in the Fig.11 and Fig.12. The air turbulence is 15.92 nm@0.1 m and 16.13 m@2 m. So the air turbulence is approximately 2.59 nm.

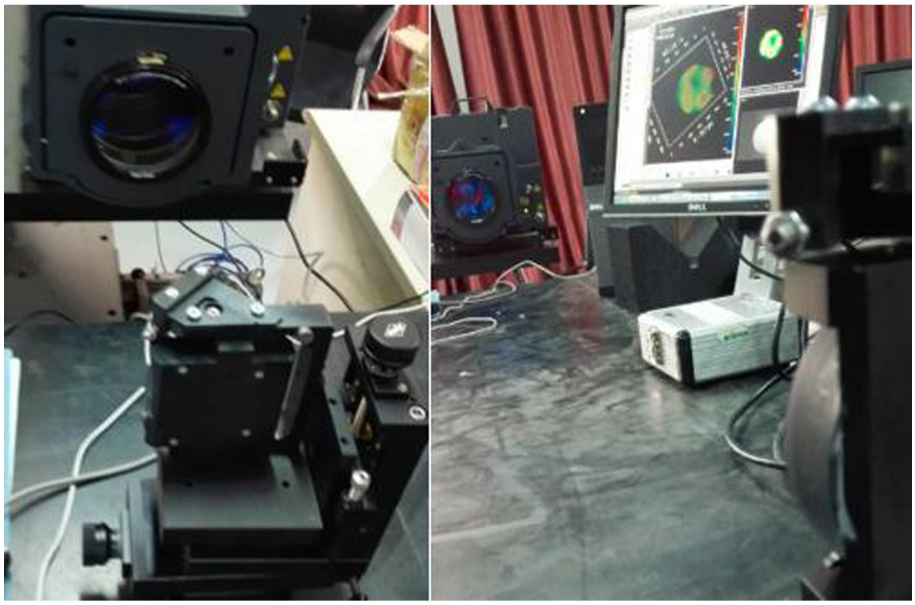

(a) Near condition (b) Far condition

Fig.11 Stitching residual error for air turbulence

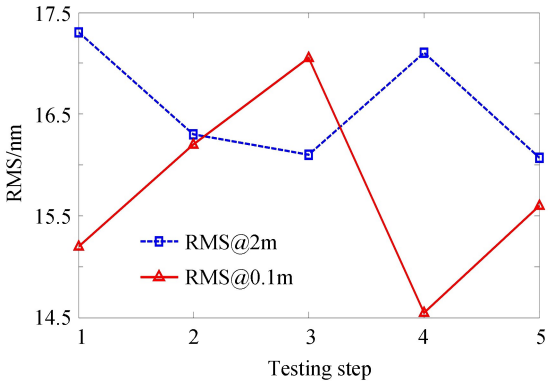

Fig.12 Stitching residual error for air turbulence

3 Numerally analysis for stitching order

Here the error involved by order of stitching will be discussed. According to the analysis in section 2, the order 1→2, 1→3, 1→4 is chosen to complete stitching. The allocation of sub apertures is shown in the left panel of Fig. 11 and the meaning of parameter is shown in the right panel of Fig. 13, where $R=1\ 000$ mm, $\rho_0=250$ mm, $f=0.8$.

Signal to Noise ratio (SNR) is a very important character for images. SNR presents the method whether involve extra error and how much it is .Stitching result (left) and residual error for white noise error (right) are shown in Fig.14. The margins between the sub apertures is not sharp. It specifies that the

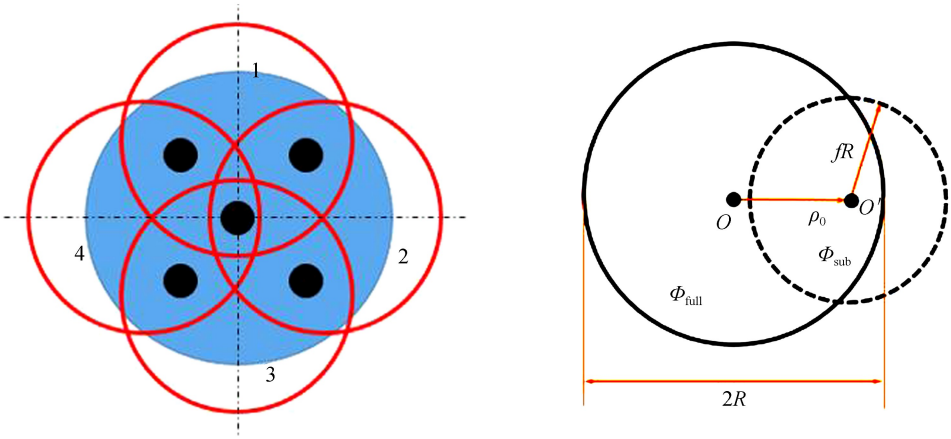

(a) Allocation of the Stitching (b) Meaning of parameter

Fig.13 Specification of stitching test

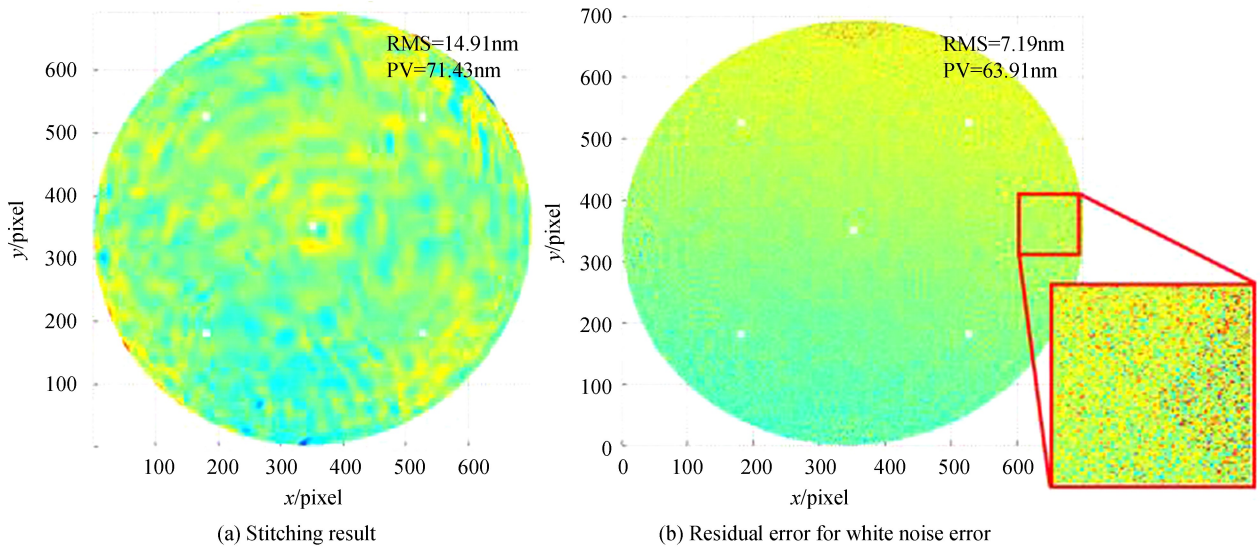

(a) Stitching result (b) Residual error for white noise error

Fig.14 Stitching result and residual error for white noise error

chosen method to do the stitching provides a good approach. The RMS of added white noise is 6.92 nm over the four aperture, averaging SNR=1.73 and the residual error is calculated as close to 7.19nm, averaging SNR=1.75. It specifies that the stitching method is sufficient to involve as little error as possible at a level of 2%.

The analysis of GSSMP sub aperture stitching error is very important in estimation of the stitching result. Stitching error analysis summary is shown in Table 4. This error analysis is mainly based on numeral analysis. When GSSMP is completed, more work on mirror figure will be processed and presented.

Table 4 Stitching error analysis summary

	Type of error	RMS of error/slope RMS	Conclusions
1	Shift	10^{-6}	Ignorable
2	Piston	10^{-6}	Ignorable
3	Tip/tilt	10^{-6}	Ignorable
4	Air turbulence	0.04 μrad	Considered
5	Stitching order	<2%	Ignorable

4 Conclusion

The analysis of GSSMP stitching error will help a lot to the design of GSSM metrology target. Practically, the mechanical accuracy contributes did not mater a lot in stitching. Middle frequency turbulence is the chief factor eliminating the performance of stitching. Any un-calibrated middle frequency error may be accumulated and enlarged with stitching steps.

References

[1] YANG Fei, LIU Guo-jun, ZHAO Hong-chao, *et al*. Stiffness allocation and analysis of TMT M3S[J]. *Editorial Office of Optics and Precision Engineering*, 2016, **24**(1): 152-159.

[2] XUE Shuai. Sub-aperture stitching test of a cylindrical mirror with large aperture[C]. Eighth International Symposium on Advanced Optical Manufacturing and Testing Technology (AOMATT2016). International Society for Optics and Photonics, 2016.

[3] SHAO Liang, ZHAO Yong-zhi, MING Ming, *et al*. Novel support for 1.2 m Zerodur primary mirror[J]. *Editorial Office of Optics and Precision Engineering*, 2016, **24**(10): 2462-2470.

[4] SMITH G A, BURGE J H. Subaperture stitching surface errors due to noise[C]. SPIE Optical Engineering + Applications. International Society for Optics and Photonics, 2015: 95750W.

[5] ZHANG P, ZHAO H, LIU B, *et al*. Simple method for the implementation of subaperture stitching interferometry[J]. *Optical Engineering*, 2011, **50**(9):

[6] ZHANG L, TIAN C, LIU D, *et al*. Non-null annular subaperture stitching interferometry for steep aspheric measurement[J]. *Applied Optics*, 2014, **53**(25): 5755-5762.

[7] ZHAO K Q, BIJASTAD T, KRISTOFFERSEN K. Error analysis of subaperture processing in 1-d ultrasound arrays[J]. *IEEE Transactions on Ultrasonics, Ferroelectrics, and Frequency Control*, 2015, **62**(4): 663-672.

[8] WANG Xiao-kun, Measurement of large off-axis convex asphere by systemic stitching testing method[J]. *Chinese Optics*, 2016, **9**(1): 130-136.

[9] ZHAO Z, ZHAO H, GU F, *et al*. Non-null testing for aspheric surfaces using elliptical sub-aperture stitching technique [J]. *Optics Express*, 2014, **22**(5): 5512-5521.

[10] XUE S, CHEN S, SHI F, *et al*. Sub-aperture stitching test of a cylindrical mirror with large aperture[C]. Eighth International Symposium on Advanced Optical Manufacturing and Testing Technology (AOMATT2016). International Society for Optics and Photonics, 2016: 96840C.

[11] HE Xu, YUAN Li. Wavefront reconstruction based on discrete sampling of sub-aperture slope[J]. *Optics and Precision Engineering*, 2016, **24**(1): 20-29.

[12] YAN F, FAN B, HOU X, *et al*. Absolute subaperture testing by multiangle averaging and Zernike polynomial fitting method[J]. *Optical Engineering*, 2013, **52**(8): 085101.

[13] CHEN S, DAI Y, LI S, *et al*. Error reductions for stitching test of large optical flats[J]. *Optics and Laser Technology*, 2012, **44**(5): 1543-1550.

[14] YAN L, WANG X, ZHEN L, *et al*. Experimental study on subaperture testing with iterative triangulation algorithm [J]. *Optics Express*, 2013, **21**(19): 22628-22644.

[15] CHEN S, DAI Y, LIS PENG X. Calculation of subaperture aspheric departure in lattice design for subaperture stitching interferometry[J]. *Optical Engineering*, 2010, **49**: 023601.

[16] MIYASHITA A, OGASAWARA R, TAKATO N, *et al*. Temperature control for the primary mirror and seeing statistics of Subaru Telescope[C]. Astronomical Telescopes and Instrumentation. International Society for Optics and Photonics, 2003: 255-263.

[17] OTSUBO M, OKADA K, TSUJIUCHI J. Measurement of large plane surface shapes by connecting small-aperture interferograms[J]. *Optical Engineering*, **33**(1994): 608-613.

[18] ZHAO Xing, ZHENG Yi, ZHANG Zan, *et al*. Characterization of freeform optical surfaces based on surface slope[J]. *Optics and Precision Engineering*, 2015, **23**(7): 1957-1964.

[19] ANGELI G Z, SEO B J, NISSLY C, *et al*. A convenient telescope performance metric for imaging through turbulence [C]. SPIE Optical Engineering+ Applications. International Society for Optics and Photonics, 2011: 812709.

[20] SUPRANOWITZ C, MCFEE C, MURPHY P. Asphere metrology using variable optical null technology[C]. 6th International Symposium on Advanced Optical Manufacturing and Testing Technologies (AOMATT 2012). International Society for Optics and Photonics, 2012: 841604.

[21] PENG Su. Absolute measurements of large mirrors[D]. The University of Arizona, 2008.